SANDIA REPORT
SAND2018-11215
Unlimited Release
Printed October 2018

Atomistic Origins of Temperature Dependent Shear Strength in 2D Materials

John F. Curry, Adam R. Hinkle, Tomas F. Babuska, Mark A. Wilson, Michael T. Dugger, Brandon A. Krick, Nicolas Argibay and Michael Chandross

Prepared by
Sandia National Laboratories
Albuquerque, New Mexico 87185 and Livermore, California 94550

Sandia National Laboratories is a multimission laboratory managed and operated by National Technology and Engineering Solutions of Sandia, LLC, a wholly owned subsidiary of Honeywell International, Inc., for the U.S. Department of Energy's National Nuclear Security Administration under contract DE-NA0003525.

Issued by Sandia National Laboratories, operated for the United States Department of Energy by National Technology and Engineering Solutions of Sandia, LLC.

Available to DOE and DOE contractors from
U.S. Department of Energy
Office of Scientific and Technical Information
P.O. Box 62
Oak Ridge, TN 37831

Telephone: (865) 576-8401
Facsimile: (865) 576-5728
E-Mail: reports@osti.gov
Online ordering: http://www.osti.gov/scitech

Available to the public from
U.S. Department of Commerce
National Technical Information Service
5301 Shawnee Rd
Alexandria, VA 22312

Telephone: (800) 553-6847
Facsimile: (703) 605-6900
E-Mail: orders@ntis.gov
Online order: https://classic.ntis.gov/help/order-methods/

SAND2018-11215
Printed October 2018
Unlimited Release

Atomistic Origins of Temperature Dependent Shear Strength in 2D Materials

John F. Curry[1], Adam R. Hinkle[2], Tomas F. Babuska[1,3], Mark A. Wilson[2], Michael T. Dugger[1], Brandon A. Krick[3], Nicolas Argibay[1], Michael Chandross[2]

[1]Materials Mechanics & Tribology Department
[2]Computational Materials & Data Science Department
Sandia National Laboratories
P. O. Box 5800
Albuquerque, New Mexico 87185-MS0889

[3]Department of Mechanical Engineering & Mechanics
Lehigh University
Bethlehem, PA, 18015, USA

Abstract

A model that predicts the macro-scale temperature-dependent interfacial shear strength of 2D materials like MoS_2 based on atomistic mechanisms and energetic barriers to sliding has been developed. Atomistic simulations were used to systematically determine the lamellar size-dependent rotation and translation energy barriers, that were used to accurately predict a broad range of experimental data. This framework provides insights about the origins of characteristic shear strengths of 2D materials.

ACKNOWLEDGMENTS

The authors thank Greg Sawyer and James Batteas for helpful discussions about temperature-dependent materials friction behavior. This work was funded by the Laboratory Directed Research and Development program at Sandia National Laboratories, a multi-mission laboratory managed and operated by National Technology and Engineering Solutions of Sandia, LLC., a wholly owned subsidiary of Honeywell International, Inc., for the U.S. Department of Energy's National Nuclear Security Administration under contract DE-NA0003525. This material is partially based upon work supported by the National Science Foundation under grant no. 1752109. Any subjective views or opinions that might be expressed in the paper do not necessarily represent the views of the U.S. Department of Energy or the United States Government.

TABLE OF CONTENTS

FIGURES

TABLES

NOMENCLATURE

Abbreviation	Definition
2D	Two Dimensional
AFM	Atomic Force Microscopy
MD	Molecular Dynamics
NEB	Nudged Elastic Band

1. INTRODUCTION

Molybdenum disulfide (MoS_2) is a lamellar solid with applications in solid lubrication[1], catalysis[2], 2D-semiconductor-based transistors[3–5], and photodetectors[6,7]. Many lamellar solids, including MoS_2, graphite, zirconium phosphates, and hexagonal boron nitride, are useful as tribological materials, since weak interactions between lamella provide easy slip planes that manifest as low friction. Because of this, understanding the inter-lamellar or interfacial physics is of fundamental and practical value. We establish a fundamental link between the molecular structure of MoS_2 and its temperature-dependent shear strength that is likely applicable to lamellar solids in general. Specifically, we calculate energy barriers for the inter-lamellar shear of MoS_2, and used this information as the basis for a simple model that accurately predicts shear strengths measured by experiments and calculated from molecular dynamics (MD) simulations over a broad range of temperatures. While the model presently predicts the temperature-dependent shear strength of MoS_2, it is envisioned that future additions to include the role of lattice defects and adsorbed species could facilitate the design of solid lubricants that are more resistant to the effects of operating environment and aging.

Regardless of deposition method, MoS_2 naturally tends to order into a nominally defect-free lamellar molecular structure when sheared, having interfacial strength and interlayer separation governed by weak van der Waals forces. Several factors are known to influence the friction of MoS_2, including environment (e.g. oxidation, humidity)[8,9], defects[10,11], crystallographic texture[12] and inter-lamellar spacing[13,14]. As an initial attempt to relate molecular structure to tribological response we focus exclusively on the shear strength of MoS_2 in inert environments, germane to many practical applications and investigations of superlubricity (i.e. friction coefficients, $\mu < 0.01$). Dienwiebel et al.[15] and Verhoeven et al.[16] previously investigated the origins of superlubricity of lamellar solids, focusing on the effects of commensurability, or atomic registry, on the friction behavior of graphene. Shear of lamellar solids in general[17–19] and MoS_2 in particular[13,14,20,21] has been investigated using MD and ab initio simulations, generally focusing on special cases such as commensurate sliding of small MoS_2 lamella[20,21], or the dynamics of MoS_2 lamella in sliding[13,14]. However, it is important to note that commensurate sliding is likely not relevant to shear of lamellar solids, as both computational[14,16,22] and experimental[15] investigations have shown that low-friction and superlubricity are associated with *incommensurate* contact.

Early theoretical models of friction developed by Eyring[23] and Prandtl[24] attempted to link fundamental notions of energy barriers and thermally activated processes to macroscopic observations of friction. These models have been further developed or modified by others to account for tribological phenomena[25–27]. Nanoscale friction experiments using atomic force microscopy (AFM) have also been described by theoretical considerations of stick-slip behavior and thermal drift. These considerations were connected to thermally activated jumps over potential energy barriers, and used to develop a model of thermolubricity at the atomic scale[28]. In this report we consider MoS_2 as an exemplar 2D material to construct a model that bridges the gap between the molecular origins of inter-lamellar sliding and macroscopic friction. We systematically calculate the energy barriers to diffusive translation and rotation as a function of the lamellar flake size and commensurability, and use these energy barriers as the basis for a predictive model of shear strength as a function of temperature.

Singer et al.[29] showed that pure MoS_2 exhibits a constant or characteristic shear strength of about 25 MPa at room temperature, with a negligible contribution from adhesion. This enabled a simplified definition of friction coefficient μ as the ratio of a characteristic shear strength S and the applied Hertzian pressure, $\mu = S / P$. While the work of Singer et al. was only performed at room temperature, multiple reports[30–34] have shown that the friction coefficient of MoS_2 changes with temperature. There is notable disagreement in these reports, attributed to the presence of minute amounts of moisture or excessive applied stress[33,34]. Although these earlier reports establish the existence of temperature-dependent friction coefficients, they do not explicitly address the connection between temperature and shear strength, a concept novel to our work. We use data from Dunckle et al.[32] as a comprehensive supplemental experimental reference, since their work provides the broadest range of temperature-dependent friction coefficient values in a clean, ultra-high vacuum environment.

2. METHODS

A comparison of experimental and simulated friction coefficients and shear strengths of MoS_2 over a range of temperatures from 25 to 300 K is presented in Fig. 1a-b, with a comparison to data from Dunckle et al.[32]. Shear strengths were extracted from the friction coefficient data of Dunckle et al. using a calculated maximum Hertzian contact pressure of 411 MPa (based on their reported forces) and applying the relationship developed in Singer et al.[29]. Our experiments are performed with a variable-temperature friction-testing apparatus[35] using commercially available 300 nm thick initially amorphous[36] magnetron-sputtered pure MoS_2 thin films (Tribologix, Golden, CO) on 440C stainless steel substrates. Counterfaces were 3.2 mm diameter 440C steel balls at 1 N contact force and 1 mm/s sliding speed. Prior to the temperature ramps the coatings were run-in to steady-state friction coefficient ($\mu \sim 0.05$ at 20°C), indicating that a thin (5-10 nm) surface film of highly-ordered and basally-oriented MoS_2 was established[1]. The effects of temperature on microstructural evolution has not been assessed. Complementary MD simulations were performed with a reactive force field[37] using a multilayered array of nanoplatelets of MoS_2 sheared between non-defective lamellae at 1 km/s (illustrated in Fig. 2a). While this shear velocity is high compared to experiments, the computational cost of this force field coupled with the large number of simulations necessary to study a wide range of temperatures (at least six different normal loads at eight different temperatures) made it a necessity.

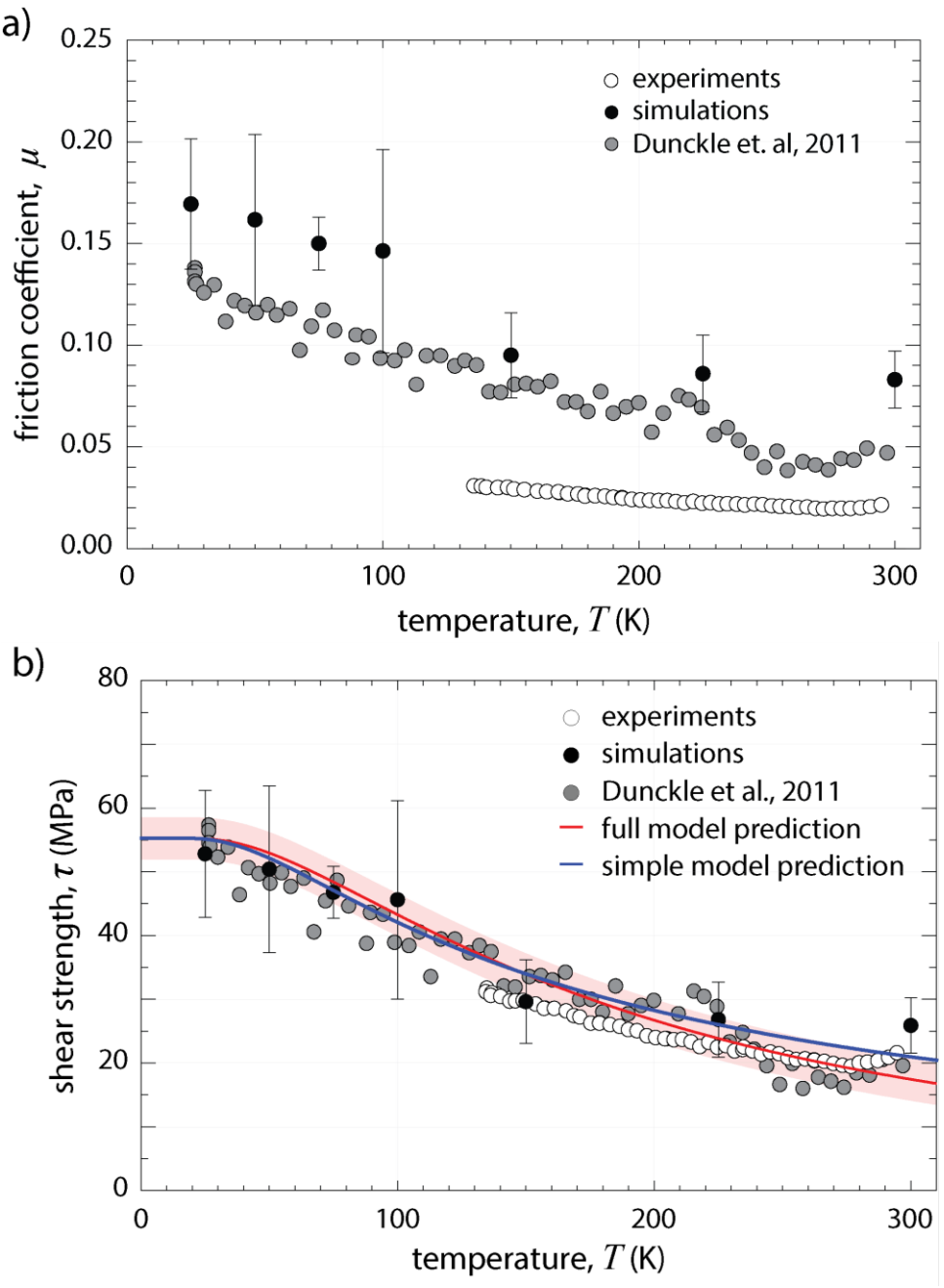

Figure 1: (a) Experimental and MD simulation measured friction coefficients as a function of temperature. (b) Overlay of experimental and simulation temperature-dependent shear strength data, full model prediction and error bounds based on uncertainty in τ_0 from simulations, and simplified model prediction based exclusively on rotation.

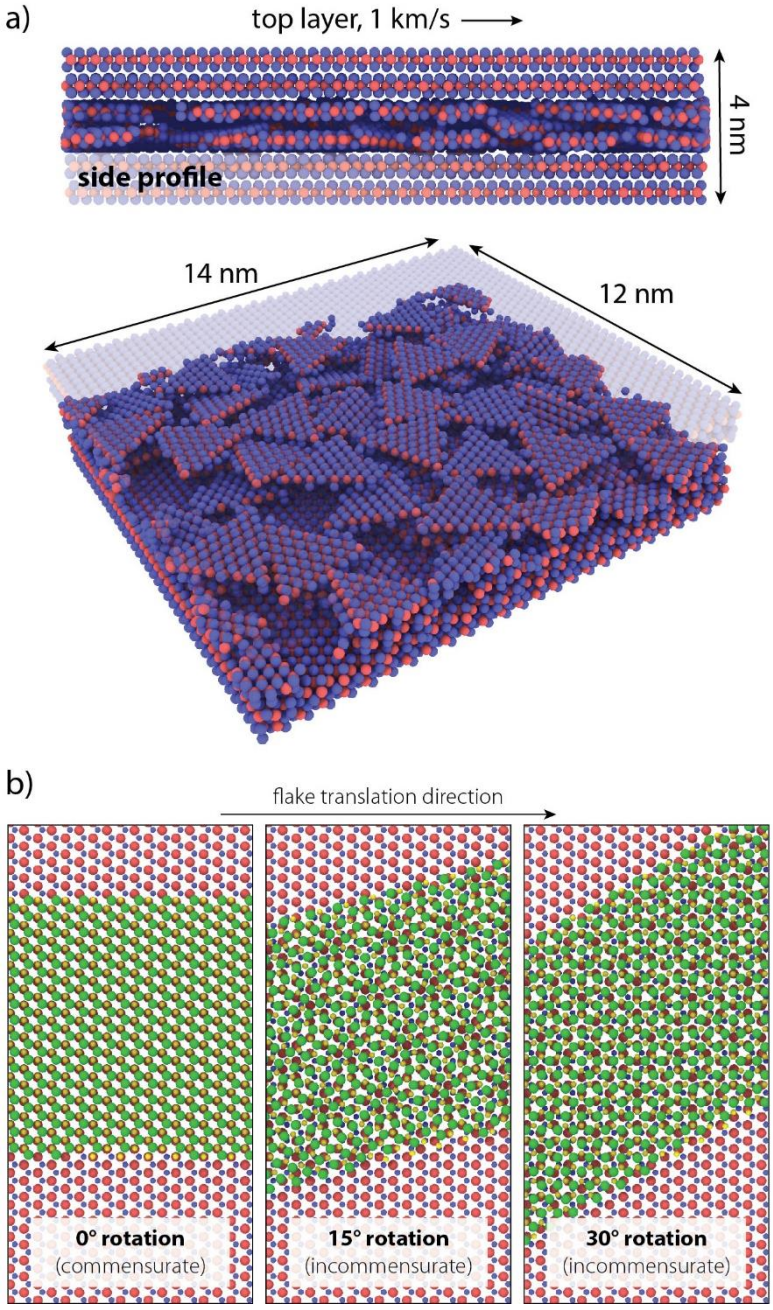

Figure 2: (a) 2D cross-sectional and sectioned 3D snapshot of MD simulations. (b) Cropped top-down views of NEB simulations for a rectangular flake sliding against an infinite, periodic MoS_2 sheet at varying degrees of rotation; these images illustrate varying degrees of registry, from commensurate to incommensurate.

Contact pressures used in experiments were within the elastic limit, justifying the use of Hertzian contact mechanics[29]. Shear strengths were calculated based on measured friction forces and Hertzian contact area calculations. Singer et al. showed that the measured friction coefficient depends on the applied load, and recent work has also shown that the friction coefficient is

temperature dependent. This motivated our use of $\tau_0 = \tau(T = 0K)$ as a material property and characteristic shear strength. We note that our measurement of $\tau(T = 300K)$ compares favorably with the value of S_0 in Singer et al. All shear strength data in Fig. 1b collapse onto a single curve, exhibiting a smooth dependence on applied temperature. The remarkable agreement between MD and experimental data suggests that nanoscale mechanisms are largely responsible for the macro-scale friction behavior. These mechanisms are revealed through a study of the energetic barriers to shear via translation and rotation of flakes.

In order to determine the energy barriers relevant to sliding, we used the nudged elastic band (NEB) method[38,39] to systematically calculate barriers to translation and rotation for a small flake of MoS_2 on top of an infinite lamellar sheet. With an understanding that shear deformation drives initially amorphous MoS_2 to form large, nominally defect-free flakes that are much larger than the sizes accessible to atomistic simulations, it was necessary to determine the dependence of these barriers as a function of flake size, and show that the normalized flake size energy barriers converged to values that can be used in the model. In Fig. 3a,c we show the results of these calculations, with barriers as a function of flake size for commensurate and incommensurate sliding. In Fig. 3b we also show the barrier to rotation of the flake, which determines the energetic penalty associated with the change from a commensurate ($\varphi = 0^o$) to a maximally incommensurate ($\varphi = 30^o$) state. Commensurability at two different rotation angles is illustrated in Fig. 2b. While even a small rotation angle away from commensurability results in low friction and incommensurate contact during sliding[14], we used 30^o as the prototypical, maximally incommensurate rotation angle. The peak energy barrier values of the converged flake sizes were found to be $E_c \cong 36.4$ meV, $E_i \cong 1.3$ meV, and $E_r \cong 12.3$ meV for commensurate sliding (E_c), incommensurate sliding (E_i), and pure rotation (E_r), respectively, with equivalent temperatures ($T_n = E_n/k_B$) provided in Table 1 and used hereafter to reference the barrier values. Our results are in reasonable agreement with previous ab initio computational determinations of commensurate MoS_2 sliding energy barriers[20,21], validating the potential and NEB approach. To the best of our knowledge, this is the first calculation of barriers to incommensurate sliding and rotation for MoS_2. We note that while we and others have found that there exist two barriers to commensurate sliding[20,21], we did not consider the larger of these barriers (1740 K) in our analysis. As previous work has shown, it is far more energetically favorable to translate along a trajectory that only requires overcoming the smaller barrier (418 K), moving between sulfur atoms rather than over them[20,21]. It is important to note that our assumptions of pure inter-lamellar sliding and the applicability of the potential energy surfaces require wear rates of the MoS_2 coatings on the order of monolayer removal per sliding pass. Wear rates greater than a monolayer per pass typically correspond to athermal friction behavior. At sufficiently low wear rates, permitting persistent surfaces, energy barriers can describe friction behavior[40]. In the temperature range 100-300 K [33], measured specific wear rates were low, with values in the range $K \cong 1\text{x}10^{-6}$ to $1\text{x}10^{-5}$ $mm^3/N\text{-}m$ (see Fig. 4); these wear rates imply that, on average, less than 1 monolayer of MoS_2 is removed per sliding pass over the duration of our experiments.

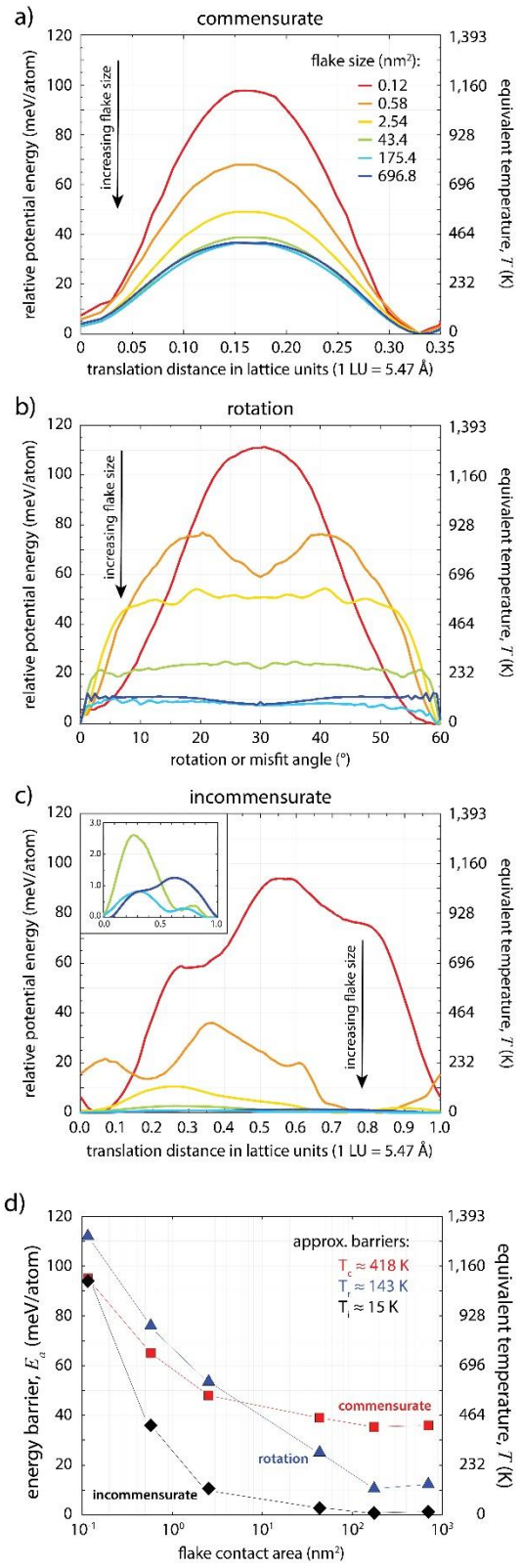

Figure 3: Flake size-dependent energy barriers for (a) translation in a commensurate state, (b) rotation, and (c) translation in the incommensurate state (at 30° rotation). (d) Summary of flake size-dependence, including equivalent temperatures.

Table 1: Summary of peak values in calculated energy barriers for a range of flake sizes. Values are presented in meV/atom and their equivalent temperature of activation.

unit cells*	contact area	incommensurate translation		pure rotation		commensurate translation	
-	nm^2	meV/atom	equiv. T (K)	meV/atom	equiv. T (K)	meV/atom	equiv. T (K)
1x1	0.12	94.0	1,090	111	1,290	96.9	1,120
2x2	0.58	36.0	418	77.0	893	67.4	782
4x4	2.54	10.5	122	54.2	628	48.6	564
16x16	43.39	2.63	30.5	25.0	290	38.5	446
32x32	175.39	0.841	9.76	10.4	120	35.4	410
64x64	701.11	1.27	14.8	12.3	143	36.1	418

* approximate number of MoS_2 unit cells comprising a flake

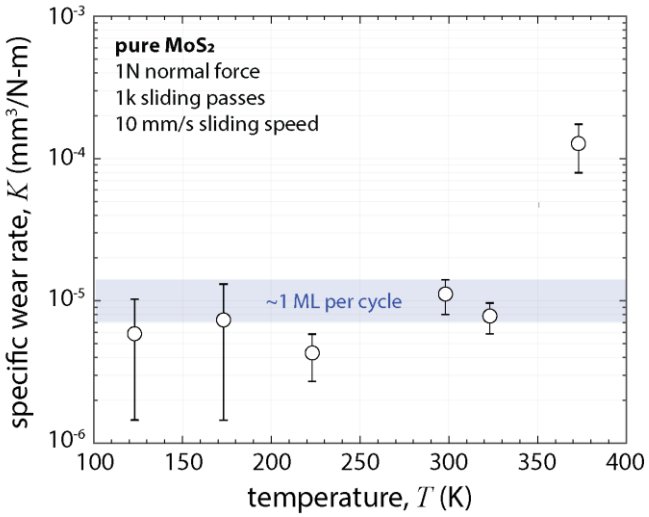

Figure 4: Temperature-dependent specific wear rates for MoS_2 films, showing monolayer/cycle wear rates in the temperature-dependent regime.

The convergence of the energy barriers with flake sizes that are still in the nanometer range, as seen in Figs. 3a-c and summarized in Fig. 3d, suggests that these values should be generally applicable across a broad range of length scales, from AFM to macro-scale experiments. The results in Fig. 3d (and summarized in Table 1) show that the incommensurate barrier to sliding is always lower than the commensurate barrier, as expected from the discussion above and prior work[20,21]. The calculated barrier to rotation, however, shows that the overall energy of the commensurate state ($\varphi = 0^o$ in Fig. 2b) is lower than that of the incommensurate state ($\varphi = 30^o$ in Fig. 2b). This result shows the importance of understanding the energetic cost to rotation from a commensurate to an incommensurate state. It also demonstrates that while there exist two energetic barriers to incommensurate sliding (i.e. the barrier to rotate to the incommensurate state and the barrier to slide in that state), the combined barrier is still lower than the barrier to commensurate sliding for large flakes. This indicates that incommensurate sliding is always the energetically preferred mechanism.

3. RESULTS & DISCUSSION

We now show that it is possible to develop a remarkably effective, yet simple model for predicting the temperature-dependent shear strength $\tau(T)$ and thus friction coefficient $\mu(T)$ of MoS_2 based on a combination of these barriers to translation and rotation. We consider two routes for accommodating shear of MoS_2 lamellae, namely commensurate and incommensurate sliding. The Arrhenius equation describes the rate of thermally overcoming an energy barrier E_n as $p_n \propto \exp\left(\frac{-E_n}{k_B T}\right) = \exp\left(\frac{-T_n}{T}\right)$, where k_B is the Boltzmann constant and T is temperature. If we consider this expression to represent a probability p_n, then the failure f_n to overcome this barrier is $f_n = 1 - p_n$. We can then write the overall probability for a flake to slide thermally as $p_{slide} = p_r p_i + f_r p_c$ where the two terms in this expression account for the likelihood that a flake must either (1) rotate from commensurate to incommensurate contact and overcome the incommensurate barrier to sliding, or (2) fail to rotate and then overcome the commensurate barrier to sliding. The expression above, written in terms of the probability to overcome barriers thermally, describes the probability of lamella sliding diffusively. Friction, however, is associated with the application of a stress to induce sliding, suggesting that we should consider the *failure* to slide thermally, written as $f_{slide} = 1 - p_{slide} = 1 - (p_r p_i + f_r p_c)$. We note that, analogous to Arrhenius rates, all terms in this expression require a pre-factor, and this factor is likely different for each probability. As we are currently unable to calculate these pre-factors, we have chosen not to include them in the individual terms, and instead group them into a single pre-factor, as shown below. We consider the shear strength of an MoS_2 film to be proportional to the failure to slide thermally, converging at $T = 0K$ to the characteristic shear strength τ_0. We can then express temperature-dependent shear strength as shown in Eq. 1.

$$\tau(T) = \tau_0 \cdot f_{slide} = \tau_0 \left[1 - \exp\left(-\frac{T_i + T_r}{T}\right) - \exp\left(-\frac{T_c}{T}\right) + \exp\left(-\frac{T_r + T_c}{T}\right) \right] \quad \text{Eq. 1}$$

By using the NEB calculated barriers for the limiting case of large flakes, shown in Fig. 3d, τ_0 is the only adjustable parameter in Eq. 1. To arrive at a predictive model with no adjustable parameters, we determined a value for τ_0 by fitting Eq. 1 (with the various T_n from the NEB calculations) to the temperature-dependent shear strength data from our MD simulations (Fig. 1b), arriving at a value of $\tau_0 = 55.3 \pm 3.1 MPa$. In Fig. 1b we show the results of this model overlaid on the experimental (from our experiments, as well as from Dunckle et al.[32]) and MD simulation data, and find remarkable quantitative agreement. We estimated error bounds for this model based on the uncertainty in the fit for τ_0 and show this range as the shaded region in Fig. 1b. For infinite sheets, the incommensurate barrier is expected to vanish[22]. Additionally, the large barrier to commensurate sliding implies that it should not play a significant role in the frictional response either. We therefore expect that the rotational barrier alone can describe the temperature-dependence of the shear strength. To demonstrate this, we remove the contribution of the incommensurate and commensurate translation barriers so that,

$$\tau(T) = \tau_0 \cdot f_{slide} \cong \tau_0 (1 - p_r) = \tau_0 \left[1 - \exp\left(-\frac{T_r}{T} \right) \right] \quad \text{Eq. 2}$$

with a single energy barrier, $T_r \cong 143K$. This simplified model is also overlaid in Fig. 1b, again using $\tau_0 = 55.3 \pm 3.1 MPa$. The accuracy of the simplified model across a broad range of temperatures reinforces our claim that commensurate sliding does not play a significant role in the tribological response of MoS_2, in contrast to prior work[20,21,41]. We expect that these effects generalize to other 2D materials (with different energy barriers), in that shear should be dominated by incommensurate sliding, and the necessity to rotate to this state from an initially incommensurate state.

The model presented in Eqs. 1 and 2 requires the use of calculated energy barriers to sliding, and we have chosen to use energy per atom in these expressions. Ignoring finite size effects (a concern at relatively small flake sizes only), as the flake size increases the total barrier to sliding increases linearly with the number of atoms (i.e. contact area). This implies that realistic (i.e. large, experimentally realized) flakes would never diffuse, and our model would lack any predictive power. A similar increase in barrier height with size also arises in the related problem of metal island diffusion[42]. In that case, however, it is found that the diffusivity of islands goes as $\exp\left(\frac{-E_a}{kT} \right) N^{\gamma}$, where E_a is an unknown, constant energy barrier, N is the number of atoms, and γ is a material-independent constant[43,44]. This expression decouples the N dependence from the exponential, and the energy per atom is a natural means to arrive at a constant value for E_a.

The contacts in MoS_2 have already been shown to be elastic, with the implication of sheets sliding over other sheets. This makes the interaction between sheets analogous to an interfacial energy, which is normalized by an area of contact. In this case, energy per atom can represent an interfacial energy, but with the correct units for use in the Arrhenius-like expressions in Eqs. 1 and 2. The use of a per-atom barrier is further justified by considering the actual motions of the atoms in both MoS_2 and the analogous case of island diffusion. In both cases, the atoms comprising the flake or island do not move as a single, bulk unit, but rather by individual edge atoms diffusing first, followed by other atoms in the bulk moving after bonds become stretched[45]. To accommodate this motion in terms of our model, we would need to consider the fraction of atoms with an energy large enough to overcome the barrier, but this would essentially imply a single-atom barrier. In our NEB calculations the flakes are not held as rigid structures, and visual inspection indicates that atoms do not move rigidly over the sulfur atoms of the substrate layer, but rather proceed via their own independent trajectories. Similar atomic-scale movement has also been considered in the motion of polymer chains[46,47], where the initial translation of individual atoms overcoming a barrier has been interpreted as slip due to dislocations at the end chains. Dislocation motion has also been discussed in the context of metal island diffusion, where it was found that islands of certain sizes diffuse more quickly than others[48] because of the size-dependent ability to support dislocations. Dislocations are known to exist in MoS_2 and other lamellar solids[49], but a study of their contribution to flake motion is beyond the scope of this work. That our model agrees so well with experimental and simulation values over the complete temperature range implies that a

rigorous theoretical justification for our energy barriers likely exists, even though at this point it is not yet fully known.

4. CONCLUSIONS

This work establishes a link between the atomistic mechanisms of inter-lamellar translation of MoS_2 and macro-scale experimentally measured shear strength. Calculations of activation energy barriers for translation and rotation of flakes were used to develop a predictive model based upon the temperature-dependent probabilities for commensurate or incommensurate sliding to occur. This model suggests that the energetic barrier to rotation is the dominant factor in the temperature-dependent friction behavior of 2D materials like MoS_2. Results from experiments and simulations are quantitatively described by this model, using a calculated value of a characteristic shear strength, τ_0. The proposed model accurately predicts friction behavior from a range of sources, including MD simulations and macro-scale experiments, and shows excellent agreement across these disparate data sets.

The model presents a basis for the development of more complex models that account for the role of compositing materials (e.g. Sb_2O_3, Au, and Ti) and environmental factors (e.g. water vapor). Such capture of the behavior of lattice defects or adsorbed species in a numerical model for shear of lamellar solids could facilitate the design of solid lubricants that are more resistant to the effects of operating environment and aging.

REFERENCES

(1) Scharf, T. W.; Prasad, S. V. *J. Mater. Sci.* **2013**, *48*, 511–531.
(2) Kibsgaard, J.; Chen, Z.; Reinecke, B. N.; Jaramillo, T. F. *Nat. Mater.* **2012**, *11*, 963–969.
(3) Shang, S. L.; Zacherl, C. L.; Fang, H. Z.; Wang, Y.; Du, Y.; Liu, Z. K. *J. Phys. Condens. Matter* **2012**, *24*, 505403.
(4) Lu, C. P.; Li, G.; Mao, J.; Wang, L. M.; Andrei, E. Y. *Nano Lett.* **2014**, *14*, 4628–4633.
(5) Radisavljevic, B.; Radenovic, A.; Brivio, J.; Giacometti, V.; Kis, A. *Nat. Nanotechnol.* **2011**, *6*, 147–150.
(6) Lopez-Sanchez, O.; Lembke, D.; Kayci, M.; Radenovic, A.; Kis, A. *Nat. Nanotechnol.* **2013**, *8*, 497–501.
(7) Sundaram, R. S.; Engel, M.; Lombardo, A.; Krupke, R.; Ferrari, A. C.; Avouris, P.; Steiner, M. *Nano Lett.* **2013**, *13*, 1416–1421.
(8) Khare, H. S.; Burris, D. L. *Tribol. Lett.* **2013**, *52*, 485–493.
(9) Khare, H. S.; Burris, D. L. *Tribol. Lett.* **2014**, *53*, 329–336.
(10) Hoffman, E. E.; Marks, L. D. *Tribol. Lett.* **2016**, *64*, 1–10.
(11) Gao, J.; Li, B.; Tan, J.; Chow, P.; Lu, T. M.; Koratkar, N. *ACS Nano* **2016**, *10*, 2628–2635.
(12) Fleischauer, P. D. *Thin Solid Films* **1987**, *154*, 309–322.
(13) Onodera, T.; Morlta, Y.; Suzuki, A.; Koyama, M.; Tsuboi, H.; Hatakeyama, N.; Endou, A.; Takaba, H.; Kubo, M.; Dassenoy, F.; Minfray, C.; Joly-Pottuz, L.; Martin, J.-M. M.; Miyamoto, A.; Morita, Y.; Suzuki, A.; Koyama, M.; Tsuboi, H.; Hatakeyama, N.; Endou, A.; Takaba, H.; Kubo, M.; Dassenoy, F.; Minfray, C.; Joly-Pottuz, L.; Martin, J.-M. M.; Miyamoto, A. *J. Phys. Chem. B* **2009**, *113*, 16526–16536.
(14) Onodera, T.; Morita, Y.; Nagumo, R.; Miura, R.; Suzuki, A.; Tsuboi, H.; Hatakeyama, N.; Endou, A.; Takaba, H.; Dassenoy, F.; Minfray, C.; Joly-Pottuz, L.; Kubo, M.; Martin, J.-M.; Miyamoto, A. *J. Phys. Chem. B* **2010**, *114*, 15832–15838.
(15) Dienwiebel, M.; Verhoeven, G. S.; Pradeep, N.; Frenken, J. W. M.; Heimberg, J. A.; Zandbergen, H. W. *Phys. Rev. Lett.* **2004**, *92*, 126101–1.
(16) Verhoeven, G. S.; Dienwiebel, M.; Frenken, J. W. M. *Phys. Rev. B - Condens. Matter Mater. Phys.* **2004**, *70*, 1–10.
(17) Gao, W.; Tkatchenko, A. *Phys. Rev. Lett.* **2015**, *114*, 1–5.
(18) Restuccia, P.; Ferrario, M.; Sivestrelli, P. L.; Mistura, G.; Righi, M. C. *Phys. Chem. Chem. Phys.* **2016**, *18*, 28997–29004.
(19) Li, S.; Li, Q.; Carpick, R. W.; Gumbsch, P.; Liu, X. Z.; Ding, X.; Sun, J.; Li, J. *Nature* **2016**, *539*, 541–545.
(20) Liang, T.; Sawyer, W. G.; Perry, S. S.; Sinnott, S. B.; Phillpot, S. R. *Phys. Rev. B* **2008**, *77*, 104105.
(21) Levita, G.; Cavaleiro, A.; Molinari, E.; Polcar, T.; Righi, M. C. *J. Phys. Chem. C* **2014**, *118*, 13809–13816.
(22) He, G.; Müser, M. H.; Robbins, M. O. *Science* **1999**, *284*, 1650–1652.
(23) Eyring, H. *J. Chem. Phys.* **1936**, *4*, 283–291.
(24) Prandtl, L.; L., P. *ZAMM - J. Appl. Math. Mech. / Zeitschrift für Angew. Math. und Mech.* **1928**, *8*, 85–106.
(25) Müser, M. H. *Phys. Rev. B - Condens. Matter Mater. Phys.* **2011**, *84*.

(26) Schallamach, A. *Proc. Phys. Soc. Sect. B* **1953**, *66*, 386.
(27) Spikes, H.; Tysoe, W. *Tribol. Lett.* **2015**, *59*, 1–14.
(28) Krylov, S. Y.; Jinesh, K. B.; Valk, H.; Dienwiebel, M.; Frenken, J. W. M. *Phys. Rev. E - Stat. Nonlinear, Soft Matter Phys.* **2005**, *71*, 1–4.
(29) Singer, I. L.; Bolster, R. N.; Wegand, J.; Fayeulle, S.; Stupp, B. C. *Appl. Phys. Lett.* **1990**, *57*, 995–997.
(30) Hamilton, M. A.; Alvarez, L. A.; Mauntler, N. A.; Argibay, N.; Colbert, R. S.; Burris, D. L.; Muratore, C.; Voevodin, A. A.; Perry, S. S.; Sawyer, W. G. *Tribol. Lett.* **2008**, *32*, 91–98.
(31) Zhao, X.; Phillpot, S. R.; Sawyer, W. G.; Sinnott, S. B.; Perry, S. S. *Phys. Rev. Lett.* **2009**, *102*, 186102.
(32) Dunckle, C. G.; Aggleton, M.; Glassman, J.; Taborek, P. *Tribol. Int.* **2011**, *44*, 1819–1826.
(33) Babuska, T. F.; Pitenis, A. A.; Jones, M. R.; Nation, B. L.; Sawyer, W. G.; Argibay, N. *Tribol. Lett.* **2016**, *63*, 1–7.
(34) Curry, J. F.; Babuska, T. F.; Brumbach, M. T.; Argibay, N. *Tribol. Lett.* **2016**, *64*, 1–5.
(35) Chandross, M.; Curry, J. F.; Babuska, T. F.; Lu, P.; Furnish, T. A.; Kustas, A. B.; Nation, B. L.; Staats, W. L.; Argibay, N. *Scr. Mater.* **2018**, *143*, 54–58.
(36) Moser, J.; Levy, F. *J. Mater. Res.* **1993**, *8*, 206–213.
(37) Vasenkov, A.; Newsome, D.; Verners, O.; Russo, M. F.; Zaharieva, R.; van Duin, A. C. T. *J. Appl. Phys.* **2012**, *112*, 13511.
(38) Henkelman, G.; Uberuaga, B. P.; Jónsson, H. *J. Chem. Phys.* **2000**, *113*, 9901–9904.
(39) Henkelman, G.; Jónsson, H. *J. Chem. Phys.* **2000**, *113*, 9978–9985.
(40) Burris, D. L.; Perry, S. S.; Sawyer, W. G. *Tribol. Lett.* **2007**, *27*, 323–328.
(41) Blumberg, A.; Keshet, U.; Zaltsman, I.; Hod, O. *J. Phys. Chem. Lett.* **2012**, *3*, 1936–1940.
(42) Shah, S. I.; Nandipati, G.; Kara, A.; Rahman, T. S. *Phys. Rev. B - Condens. Matter Mater. Phys.* **2013**, *88*, 33–36.
(43) Karim, A.; Kara, A.; Trushin, O.; Rahman, T. S. *J. Phys. Condens. Matter* **2011**, *23*.
(44) Voter, A. F. *Phys. Rev. B* **1986**, *34*, 6819–6829.
(45) Uche, O. U.; Perez, D.; Voter, A. F.; Hamilton, J. C. *Phys. Rev. Lett.* **2009**, *103*, 1–4.
(46) Dong, H.; Wang, Z.; O'Connor, T. C.; Azoug, A.; Robbins, M. O.; Nguyen, T. D. *J. Mech. Phys. Solids* **2018**, *116*, 70–98.
(47) O'Connor, T. C.; Robbins, M. O. *ACS Macro Lett.* **2016**, *5*, 263–267.
(48) Hamilton, J. C. *Phys. Rev. Lett.* **1996**, *77*, 885–888.
(49) Yazyev, O. V.; Louie, S. G. *Phys. Rev. B - Condens. Matter Mater. Phys.* **2010**, *81*, 1–7.

DISTRIBUTION

2	Department of Mechanical Engineering & Mechanics (electronic copy) Attn: B. Krick, T. Babuska Lehigh University Bethlehem, PA, 18015, USA		
1	MS0889	N. Argibay	1851 (electronic copy)
1	MS0889	M.E. Chandross	1864 (electronic copy)
1	MS0889	J.F. Curry	1851 (electronic copy)
1	MS0889	M.T. Dugger	1851 (electronic copy)
1	MS0889	A.R. Hinkle	1864 (electronic copy)
1	MS0889	R.P. Muller	1864 (electronic copy)
1	MS0889	M.A. Wilson	1864 (electronic copy)
1	MS0889	C.D. Yarrington	1851 (electronic copy)
1	MS0899	Technical Library	9536 (electronic copy)
1	MS0359	D. Chavez, LDRD Office	1911 (electronic copy)


Sandia National Laboratories